VISUAL INTERPRETATION OF CYLINDRICAL DEFORMATION

- A Sideways Look At Contour Motion!

R.M.Cameron-Jones

Department of Artificial Intelligence
University of Edinburgh

This paper presents a new technique for the interpretation of the changing intensity image generated by a cylindrical Lambertian surface undergoing a stretching motion, such that it may be regarded as a deforming curve in a plane. The method, based around the rate of intensity change, uses a regularisation-style approach to estimate the tangential and normal velocities along the surface, assuming knowledge of the initial surface structure and the motion of the endpoints.

1. Introduction

Most computer vision research is concerned with rigid surfaces, whether static or moving. Motion research has usually assumed either that the object is strongly textured, or that the shading remains unaltered under motion. This paper presents work using the different assumption of Lambertian reflectance, as often assumed in shape from shading techniques, to enable the interpretation of a simplified case of non-rigid surface motion - a reduced dimension case, in which the surface motion may be considered to be that of a curve in a plane.

Presentation of the new method will be preceded by a description of other computer vision work involving non-rigid surfaces.

2. Previous Non-rigid Object Research

Subbarao[1], Ullman[2], Koenderink and van Doorn[3], Chen and Penna[4] and Terzopolous *et al*[5] have all addressed different low/middle-level problems within non-rigid vision, under varying assumptions.

Subbarao's work considers the 2D image flow due to a deforming surface viewed under perspective projection. It is suggested how the general principle of using Taylor series expansions (in space and time) of both image flow and surface patch, as per the rigid motion analysis presented, may be extended to the case of "arbitrarily time-varying 3D scenes".

Ullman's work considers the case of a discrete time sequence of images, under orthographic projection, containing corresponded tokens. For each new image a 3-D structure (initially flat) is hypothesised based on an optimisation process which minimises the sum of the squares of changes in 3-D inter-token distances between images. When this method works for a rigid structure the hypotheses converge on the true structure or its reflection about the image plane - equally valid solutions under orthographic projection. The method admits the possibility of calculating non-rigid structures in motion, but even for rigid structures the rate of convergence is highly dependent on the amount by which the viewpoint changes between images. It is of course reasonable to have problems when the sampling rate is inadequate relative to the motion, but less acceptable may be the instability in the limiting continuous time case illustrated by Grzywacz and Hildreth[6] in their paper based on Ullman's method.

Koenderink and van Doorn's work considers the case of point motion in continuous time, under perspective projection, where the points are assumed to be on a surface undergoing a bending (isometric) motion. This is approximated, using a difference geometry approach, by hinged planar facets, and the constraints on the motion at a single vertex considered. It is shown that partial shape information (with a relief ambiguity) may be recovered from the point motions and derived estimates of differential invariants of the motion field.

Chen and Penna's work considers the case of two corresponded images under perspective projection of the same surface, which has undergone an isometric transformation between images. A Taylor series expansion for the 3-D surface motion around any point is then recovered from the correspondence, the equations of the projection, and surface shape information (nominally recovered by three source photometric stereo).

Terzopolous *et al* consider a discrete time series of stereo image pairs of a deforming object. The occluding contours are used to constrain the shape of a symmetry-seeking deformable model (with motion damping); thus

Acknowledgement :
The author wishes to thank Drs. R.B.Fisher and J.C.T.Hallam for supervision, L.D.Cai and A.K.Robertson also of the department for technical and other comments, Drs. B.F.Buxton and D.W.Murray of GEC Hirst for their suggestions and the SERC for financial support.

AVC 1988 doi:10.5244/C.2.21

instantaneous shape and non-rigid motion are recovered. It is intended to extend the method to use other constraints, such as reflectivity.

3. Interpretation of Cylindrical Stretching Motion

Consider an arbitrarily smoothly deforming Lambertian surface viewed under orthographic projection from the x direction, as illustrated in figure 1.

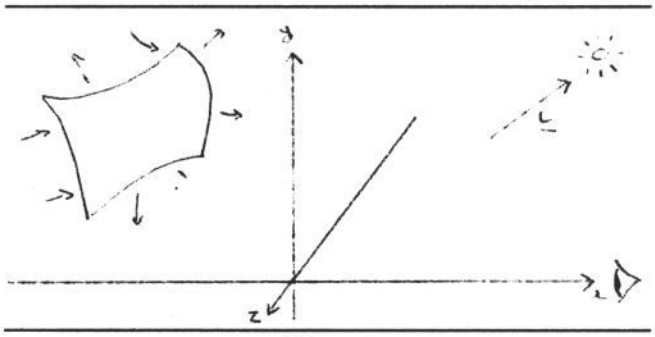

Figure 1

It will be shown how the expression for the change in intensity in the image due to surface motion may be used under certain assumptions to directly provide estimates of components of the surface velocity. As the temporal derivatives would normally be found from differencing discrete time images, an alternative to the proposed method would be to calculate the surface structure explicitly for each image, then calculate a correspondence to estimate the velocities.

For a Lambertian surface, the image intensity corresponding to a point on the surface, will be :

$$I = \rho \, \underline{l} \cdot \underline{n} \tag{1}$$

where
I = image intensity (assuming appropriate sensor calibration)
ρ = surface albedo, hereafter absorbed into $\underline{l}$ for convenience
$\underline{l}$ = light source vector
$\underline{n}$ = unit normal vector on the surface

Assuming the albedo to be unaffected in a motion, the change in intensity at the (changing) image point corresponding to a given point on the surface is :

$$\underline{l} \cdot \left[\underline{\omega} \times \underline{n} \right] \tag{2}$$

where the vector fields $\underline{\omega}$ (angular velocity), and $\underline{n}$ are defined on the surface, as is $\underline{v}$ (translational velocity).

Considering a fixed image point, the change in intensity is:

$$\dot{I} = -(\nabla I \cdot \underline{v}) + \underline{l} \cdot \left[\underline{\omega} \times \underline{n} \right] \tag{3}$$

where
the dot notation (eg $\dot{\alpha}$) is used for differentiation wrt time.
∇I represents the 3-D gradient of the intensity.

The above contains reference to $\underline{\omega}$, which may be re-expressed in terms of spatial derivatives of the velocity field as follows (from Weatherburn[7,8]) :

$$\underline{\omega} = \nabla \times \underline{v} - \frac{1}{2} \left[\underline{n} \cdot \left[\nabla \times \underline{v} \right] \right] \underline{n} \tag{4a}$$

hence:

$$\underline{\omega} \times \underline{n} = \left[\nabla \times \underline{v} \right] \times \underline{n} \tag{4b}$$

where for any vector field $\underline{\theta}$, defined on a surface $\underline{r}$ parameterised in terms of α and β, letting $\underline{\theta}_1$ denote $\frac{\partial \underline{\theta}}{\partial \alpha}$ and $\underline{\theta}_2$ denote $\frac{\partial \underline{\theta}}{\partial \beta}$, and similarly for $\underline{r}_1$ and $\underline{r}_2$:

$$\nabla \times \underline{\theta} = \tag{5}$$

$$H^{-2} \left[\underline{r}_1 \times \left[G \, \underline{\theta}_1 - F \, \underline{\theta}_2 \right] + \underline{r}_2 \times \left[E \, \underline{\theta}_2 - F \, \underline{\theta}_1 \right] \right]$$

where

$$E = \underline{r}_1^{\,2} \tag{6a}$$

$$F = \underline{r}_1 \cdot \underline{r}_2 \tag{6b}$$

$$G = \underline{r}_2^{\,2} \tag{6c}$$

$$H = \sqrt{E\,G - F^2} \tag{6d}$$

E, F and G are the coefficients of the first fundamental form, and the integral of H gives the area of a region. If we assume the surface is parameterised in terms of its (unit speed) lines of curvature, F is zero, and E,G and H are all unity. Thus:

$$\nabla \times \underline{\theta} = \left[\underline{r}_1 \times \underline{\theta}_1 + \underline{r}_2 \times \underline{\theta}_2 \right] \tag{7}$$

Analysis of this general case is the author's current research topic, but this paper continues with the reduced dimension special case where the surface is moving so as to be cylindrical, with the generators aligned with the z-axis, the surface may be considered to be a curve in motion in x and y, (hence the paper's subtitle), see figure 2.

Thus, the curl of the velocity field is given by:

$$\nabla \times \underline{v} = \frac{\partial \underline{r}}{\partial s} \times \frac{\partial \underline{v}}{\partial s} \tag{8a}$$

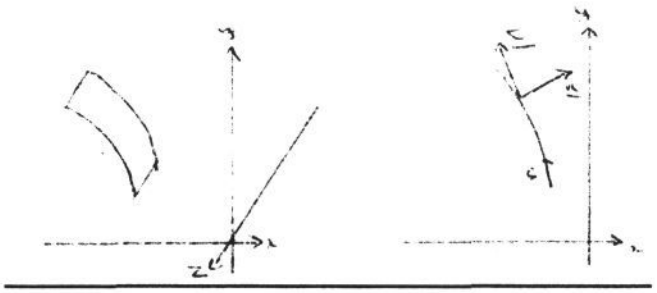

Figure 2

where s is the arc-length, hence:

$$\nabla \times \underline{v} = \underline{t} \times \frac{\partial \underline{v}}{\partial s} \tag{8b}$$

Hence, from (3),(4b) and (8b) :

$$\dot{I} = -(\nabla I \cdot \underline{v}) + \underline{l} \cdot \left[\left[\frac{\partial \underline{r}}{\partial s} \times \frac{\partial \underline{v}}{\partial s} \right] \times \underline{n} \right] \tag{9}$$

Considering the normal component of $\frac{\partial \underline{v}}{\partial s}$, this can be evaluated as follows :

$$\underline{v} = v_t \, \underline{t} + v_n \, \underline{n} \tag{10a}$$

hence

$$\frac{\partial \underline{v}}{\partial s} = \frac{\partial v_t}{\partial s} \underline{t} + v_t \frac{\partial \underline{t}}{\partial s} + \frac{\partial v_n}{\partial s} \underline{n} + v_n \frac{\partial \underline{n}}{\partial s} \tag{10b}$$

thus from the Frenet relations:

$$\frac{\partial \underline{v}}{\partial s} \cdot \underline{n} = v_t \, \kappa + \frac{\partial v_n}{\partial s} \tag{10c}$$

and, from (9) and (10c), evaluating the vector triple product gives:

$$\dot{I} = -(\nabla I \cdot \underline{v}) - \underline{l} \cdot \left[\left[v_t \, \kappa + \frac{\partial v_n}{\partial s} \right] \underline{t} \right] \tag{11}$$

which may be expanded in terms of tangential and normal components of velocity as :

$$\dot{I} + I_t \, v_t + I_n \, v_n + \kappa \, l_t \, v_t + l_t \frac{\partial v_n}{\partial s} = 0 \tag{12}$$

where I_t and I_n represent the respective components of the intensity gradient in the plane, (recall that I_x and I_z are zero).

This equation may be simplified further by considering the coefficients of v_t :

$$I_t = \frac{\partial}{\partial s} (\underline{l} \cdot \underline{n}) = -\kappa \, l_t \tag{13}$$

hence

$$\dot{I} + I_n \, v_n + l_t \frac{\partial v_n}{\partial s} = 0 \tag{14}$$

Clearly if this equation were used to attempt to solve for the velocity of the surface, assuming all other quantities known from a static analysis (eg shape from shading and stereo contour[9]), the determination of the velocity would be "ill-posed" as the equation imposes no constraint upon v_t. Hence analogously to the problem of contour motion considered by Hildreth[10], a further constraint must be introduced. As the stretching of the arc is that in the physical world, not that of the image, the method of stretch-minimising, (as opposed to say velocity smoothness), is used. This is done in the standard regularisation framework (see eg [11,12]), v_t and v_n being determined to minimise the following, where λ is the regularisation parameter :

$$\int \left[\dot{I} + I_n \, v_n + l_t \frac{\partial v_n}{\partial s} \right]^2 + \lambda \left[\frac{\partial \underline{v}}{\partial s} \cdot \underline{t} \right]^2 d \, s \tag{15}$$

or substituting for $\frac{\partial \underline{v}}{\partial s} \cdot \underline{t}$ (from eq 17b):

$$\int \left[\dot{I} + I_n \, v_n + l_t \frac{\partial v_n}{\partial s} \right]^2 + \lambda \left[\frac{\partial v_t}{\partial s} - \kappa \, v_n \right]^2 d \, s \tag{16}$$

This expression can be minimised directly using numerical methods, as may be preferable in practice, alternatively formally minimising such an integral is a problem in the calculus of variations, (see eg Stephenson[13]). Minimising $\int f \left[x, y, y' \right] dx$, (where y' is the differential of y with respect to x) yields the Euler equation :

$$\frac{\partial f}{\partial y} - \frac{d}{dx} \left[\frac{\partial f}{\partial y'} \right] = 0 \tag{17}$$

Applying this to (16), minimising with respect to v_t and v_n respectively gives :

$$\frac{\partial}{\partial s} \lambda \left[\frac{\partial v_t}{\partial s} - \kappa \, v_n \right] = 0 \tag{18a}$$

and

$$I_n \left[\dot{I} + I_n \, v_n + l_t \frac{\partial v_n}{\partial s} \right] - \kappa \, \lambda \left[\frac{\partial v_t}{\partial s} - \kappa \, v_n \right] - \frac{\partial}{\partial s} \left[l_t \left[\dot{I} + I_n \, v_n + l_t \frac{\partial v_n}{\partial s} \right] \right] = 0 \tag{18b}$$

hence

$$\left[\frac{\partial^2 v_t}{\partial s^2} - \frac{\partial \kappa}{\partial s} v_n - \kappa \frac{\partial v_n}{\partial s} \right] = 0 \qquad (19a)$$

and

$$I_n \left[\dot{I} + I_n v_n + l_t \frac{\partial v_n}{\partial s} \right] - \kappa \lambda \left[\frac{\partial v_t}{\partial s} - \kappa v_n \right] \qquad (19b)$$

$$- l_t \left[\frac{\partial \dot{I}}{\partial s} + \frac{\partial I_n}{\partial s} v_n + \left[I_n + \frac{\partial l_t}{\partial s} \right] \frac{\partial v_n}{\partial s} + l_t \frac{\partial^2 v_n}{\partial s^2} \right] = 0$$

This is a pair of coupled second order partial differential equations (PDEs) in v_t and v_n, for which a numerical method of solution may be attempted, given the boundary values of v_t and v_n. The use of central finite difference approximations leads to a sparse system of linear equations, which would be best solved by a method exploiting the near-diagonal form; however a more general partial pivoting method (from Conte and de Boor[14]) was used in the implementation to allow for the possible use of other types of constraint, which might change the structure of the equations.

Two test cases were tried on perfect data, ie the value of all the coefficients (I_n $\dot{I}$ etc) in the PDEs was assumed to be exactly known, as were the end velocities (obtainable from eg stereo-motion). These tests constitute only a check on the analysis - they are far from an application of the method to real image data. The cases both consisted of a circular arc, (representing a circular cylinder), moving so as to remain circular. In the first case the arc bends without stretching, in the second it stretches uniformly without changing curvature, see figure 3.

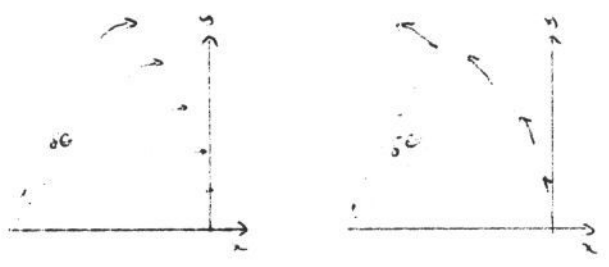

Figure 3 : Bending and stretching arcs -
$\delta\theta$ is the angle increment between points on the arc

The numerical results from two examples of each case are presented in the Appendix. The examples of bending motion illustrate that as the correct value of the regularising term is zero, the solution found matches the true velocity. The examples of uniform stretch show that the solution found tends to the true velocity as the regularising parameter is decreased, causing the method to become similar to minimising the stretch term subject to the intensity change equation as a constraint, when the uniform stretch case should be solved correctly.

Preliminary tests of the method on synthetic data representing the discrete time and quantised noisy measurements inherent in machine vision systems suggest that the use of regularisation has resulted in a method which doesn't "blow up" the errors excessively. However, even the basic input of intensity rate is not usually measured accurately and the method relies upon measurement of such quantities as surface curvature, the accurate estimation of which remains a research topic. The range of surface smoothing and fitting techniques currently being developed by other workers (eg L.D.Cai in this department) may at least improve performance in the measurement of such quantities. Note that the third order differential term $\frac{\partial \kappa}{\partial s}$ is a result of the problem being solved in terms of v_t and v_n, rephrasing for v_x and v_y eliminates this term.

4. Conclusions

It has been shown how consideration of the intensity change induced by a Lambertian surface in motion leads to a restriction upon the possible motion giving rise to that changing intensity pattern. This restriction, combined with an assumption of stretch minimisation has allowed the estimation of surface velocities for the (suitably viewed) case of cylindrical motion. Given perfect input data, these estimates match the true velocities in such important cases as pure bending motion, and uniform stretching motion.

5. Bibliography

1. Subbarao,M. : 1986 : "Interpretation of image motion fields : A spatio-temporal approach", in Proceedings of IEEE Workshop on Motion Representaion and Analysis 1986.

2. Ullman,S. : 1984 : "Maximising Rigidity : the incremental recovery of 3-D structure from rigid and nonrigid motion", in Perception Vol 13 pp 255-274.

3. Koenderink,J.J. and van Doorn,A.J. : 1986 : "Depth and shape from differential perspective in the presence of bending deformations" in J.Opt.Soc.Am.A Vol.3 No.2.

4. Chen,S. and Penna,M. : 1986 : "Shape and Motion of Nonrigid Bodies" in Computer Vision Graphics and Image Processing (CVGIP) Vol. 36.

5. Terzopolous,D. , Witkin,A. , Kass, M. : 1987 : "Energy constraints on deformable bodies : Recovering shape and non-rigid motion" in Proceedings of AAAI 1987.

6. Grzywacz,N.M. and Hildreth,E.C. : 1987 : "Incremental rigidity scheme for recovering structure

from motion : position-based versus velocity-based formulations" in J.Opt.Soc.Am.A Vol.4 No.3 .

7. Weatherburn,C.E. : 1931 : "Differential geometry of three dimensions: volume 1" Cambridge University Press.

8. Weatherburn,C.E. : 1930 : "Differential geometry of three dimensions: volume 2" Cambridge University Press.

9. Blake,A. , Zisserman,A. and Knowles,G. : 1985 : "Surface descriptions from stereo and shading" in Image and Vision Computing Vol. 3 No. 4.

10. Hildreth,E.C. : 1984 : "The Measurement of Visual Motion" MIT Press.

11. Tikhonov,A.N. and Arsenin,V.Y. : 1977 : "Solutions of Ill-Posed Problems" Winston and Sons.

12. Bertero,M. , Poggio,T. and Torre,V. : 1987 : "Ill-posed problems in early vision", MIT AI Memo 924.

13. Stephenson,G. : 1973 : "Mathematical Methods for Science Students", Longman.

14. Conte,S.D. and de Boor,C. : 1981 : "Elementary Numerical Analysis" McGraw-Hill.

Appendix

Bending Motion - First Example

l_x 0.7071, l_y 0.7071, ρ 1.0
radius 1.0, radius rate 1.0, λ 1.0, δθ 0.01

Tangential velocity solution:

Theta	estimate	true
-4.00e-02	1.0666e-05	1.0666e-05
-3.00e-02	4.5001e-06	4.4998e-06
-2.00e-02	1.3336e-06	1.3333e-06
-1.00e-02	1.6682e-07	1.6667e-07
0.00e+00	2.7137e-11	0.0000e+00
1.00e-02	-1.6677e-07	-1.6667e-07
2.00e-02	-1.3335e-06	-1.3333e-06
3.00e-02	-4.5001e-06	-4.4998e-06
4.00e-02	-1.0666e-05	-1.0666e-05

Normal velocity solution:

Theta	estimate	true
-4.00e-02	7.9990e-04	7.9989e-04
-3.00e-02	4.4999e-04	4.4997e-04
-2.00e-02	2.0002e-04	1.9999e-04
-1.00e-02	5.0029e-05	5.0000e-05
0.00e+00	3.1309e-08	0.0000e+00
1.00e-02	5.0030e-05	5.0000e-05
2.00e-02	2.0002e-04	1.9999e-04
3.00e-02	4.4999e-04	4.4997e-04
4.00e-02	7.9991e-04	7.9989e-04

Bending Motion - Second Example

l_x 0.866, l_y 0.5, ρ 2.0, radius 0.5
radius rate 3.0, λ 0.1, δθ 0.02

Tangential velocity solution:

Theta	estimate	true
-8.00e-02	2.5592e-04	2.5592e-04
-6.00e-02	1.0798e-04	1.0798e-04
-4.00e-02	3.1999e-05	3.1997e-05
-2.00e-02	4.0016e-06	3.9999e-06
0.00e+00	1.1335e-09	0.0000e+00
2.00e-02	-3.9995e-06	-3.9999e-06
4.00e-02	-3.1998e-05	-3.1997e-05
6.00e-02	-1.0798e-04	-1.0798e-04
8.00e-02	-2.5592e-04	-2.5592e-04

Normal velocity solution:

Theta	estimate	true
-8.00e-02	9.5947e-03	9.5949e-03
-6.00e-02	5.3981e-03	5.3984e-03
-4.00e-02	2.3993e-03	2.3997e-03
-2.00e-02	5.9959e-04	5.9998e-04
0.00e+00	-3.9759e-07	0.0000e+00
2.00e-02	5.9961e-04	5.9998e-04
4.00e-02	2.3994e-03	2.3997e-03
6.00e-02	5.3981e-03	5.3984e-03
8.00e-02	9.5948e-03	9.5949e-03

Stretching case - First Example

l_x 0.7071, l_y 0.7071, ρ 1.0, radius 1.0
extension rate 1.0, λ 1.0, δθ 0.01

Tangential velocity solution:

Theta	estimate	true
-4.00e-02	-4.0012e-02	-4.0000e-02
-3.00e-02	-3.0017e-02	-3.0000e-02
-2.00e-02	-2.0015e-02	-2.0000e-02
-1.00e-02	-1.0009e-02	-1.0000e-02
0.00e+00	-1.5029e-06	0.0000e+00
1.00e-02	1.0007e-02	1.0000e-02
2.00e-02	2.0013e-02	2.0000e-02
3.00e-02	3.0015e-02	3.0000e-02
4.00e-02	4.0012e-02	4.0000e-02

Normal velocity solution:

Theta	estimate	true
-4.00e-02	-8.6663e-04	0.0000e+00
-3.00e-02	-1.5555e-03	0.0000e+00
-2.00e-02	-2.0614e-03	0.0000e+00
-1.00e-02	-2.3791e-03	0.0000e+00
0.00e+00	-2.5029e-03	0.0000e+00
1.00e-02	-2.4271e-03	0.0000e+00
2.00e-02	-2.1455e-03	0.0000e+00
3.00e-02	-1.6517e-03	0.0000e+00
4.00e-02	-9.3885e-04	0.0000e+00

Stretching case - Second Example

l_x 0.7071, l_y 0.7071, ρ 1.0, radius 1.0
extension rate 1.0, λ 1.0 x 10^{-10}, δθ 0.01

Tangential velocity solution:

Theta	estimate	true
-4.00e-02	-4.0000e-02	-4.0000e-02
-3.00e-02	-3.0000e-02	-3.0000e-02
-2.00e-02	-2.0000e-02	-2.0000e-02
-1.00e-02	-1.0000e-02	-1.0000e-02
0.00e+00	-1.4311e-16	0.0000e+00
1.00e-02	1.0000e-02	1.0000e-02
2.00e-02	2.0000e-02	2.0000e-02
3.00e-02	3.0000e-02	3.0000e-02
4.00e-02	4.0000e-02	4.0000e-02

Normal velocity solution:

Theta	estimate	true
-4.00e-02	-8.6810e-14	0.0000e+00
-3.00e-02	-1.5581e-13	0.0000e+00
-2.00e-02	-2.0649e-13	0.0000e+00
-1.00e-02	-2.3831e-13	0.0000e+00
0.00e+00	-2.5072e-13	0.0000e+00
1.00e-02	-2.4312e-13	0.0000e+00
2.00e-02	-2.1492e-13	0.0000e+00
3.00e-02	-1.6545e-13	0.0000e+00
4.00e-02	-9.4045e-14	0.0000e+00